Alternative blends of CO_2 for transcritical refrigeration systems. Experimental approach and energy analysis

D. Sánchez [*], F. Vidan-Falomir, L. Nebot-Andrés, R. Llopis, R. Cabello

Jaume I University, Dep. of Mechanical Engineering and Construction, Campus de Riu Sec s/n E-12071, Castellón, Spain

ABSTRACT

As a natural refrigerant, Carbon Dioxide (CO_2) has been extended in almost all refrigeration fields due to its environmental friendliness, high availability, and high technological development in the main components of the cycle. However, despite the benefits, CO_2 is limited to high-capacity applications due to the cost of components and the complex cycle arrangements to overcome the low coefficient of performance (COP) at high ambient temperatures. A simple but effective method to solve this issue involves mixing CO_2 with other refrigerants obtaining a new refrigerant mixture with higher critical points, lower working pressures and low global warming potential (GWP). Depending on the mixture percentage, the mixture flammability can be suppressed, and the performance of the refrigeration plant can be increased.

Building on this, this work determines theoretically different CO_2-based zeotropic blends as an alternative to pure CO_2 with the restrictions of non-flammability, GWP below 150 and higher COP than pure CO_2. The results suggest two blends of CO_2/R1270 and CO_2/R32 that have been prepared and energetically tested in a vertical display cooler using pure CO_2 as a reference. The results revealed that CO_2-blends reduce energy consumption by up to 17.2 % at the ambient temperature of 25 °C and up to 12.2 % at 30 °C. Moreover, the results with CO_2-blends were closest to those obtained with pure R1270 and better than R134a under the same operating conditions.

1. Introduction

Currently, the importance of the refrigeration industry in the worldwide economy and nutrition is contradicted by its relevant environmental impact because its significant contribution to greenhouse gas emissions accounted for 7.8 % in 2014 [1]. Due to this, in 2014, the European Commission put in place regulation No 517/2014 to control the massive utilization of high-GWP hydrofluocarbons (HFCs) as refrigerants and blowing agents. This regulation got into force in 2015 and established a schedule limiting the total amount of HFCs that can be put on the market and restricting their use in different refrigeration applications. In 2016, this guideline was extrapolated globally with the Kigali amendment to the Montreal Protocol (1987), which came into force in 2019, adopting a similar phase-down schedule for HFCs.

The main consequence of HFCs limitations was using alternative refrigerants with GWP below 150, such as natural refrigerants, pure hydrofluoroolefins (HFOs) or mixtures [2–5]. However, most of these substances are classified as A2L, A2 or even A3 by the ASHRAE Standard 34. Therefore, they are flammable fluids that are a feasible solution for low-charge hermetic sealed systems but not a safe alternative in medium or large refrigeration systems, except for indirect systems using secondary fluids [6]. In these conditions, CO_2 has been established as a clear alternative due to its non-flammability, high availability and relatively good transport and heat transfer properties compared with the other synthetic fluids [7]. Nevertheless, its low critical temperature has forced the adoption of complex cycle arrangements to overcome the COP reduction, especially at high ambient temperatures. Some of these configurations correspond to the flash-gas by-pass valve [8,9], the suction-to-liquid heat-exchanger (SLHX or IHX) [10], the parallel compressor [11,12], the use of ejectors [13,14], or the adoption of different subcooling systems at the exit of the gas-cooler [15–17]. However, adopting any approach inevitably increases the complexity and the cost that only large capacity systems can afford but not medium-small applications. For this later, IHX is commonly preferred for mobile air conditioning [18], beverage coolers [19] or residential air-conditioning [20], among others.

A simple but effective method to solve this issue involves mixing CO_2 with other refrigerants obtaining a zeotropic refrigerant mixture with a higher critical point, lower working pressures and low GWP. This

---

* Corresponding author.
E-mail address: sanchezd@uji.es (D. Sánchez).

Nomenclature

COP	coefficient of performance
CH	central heating
D	duty-cycle (%)
DHW	domestic hot water
E	energy (kW·h)
FIP	Fuel Inertization Point
GWP	Global Warming Potential
h	specific enthalpy (kJ·kg^{-1})
HC	HydroCarbon
HFC	HydroFluoroCarbon
HP	High-Pressure side
HT	High-Temperature cycle
IHX	Internal Heat Exchanger
LFL	Lower Flammability Limit (%)
LMTD	Logarithmic Mean Temperature Difference (K)
LT	Low-Temperature cycle
$\dot{m}$	mass flow rate (kg·s^{-1})
m	refrigerant mass charge (g)
N	compressor rotation speed (rpm)
NBP	Normal Boiling Point (°C)
P	pressure (bar)
$\dot{Q}$	heat transfer rate (W)
RH	relative humidity (%)
SH	superheating (K)
t	Time (s)
T	temperature (°C)
UFL	Upper Flammability Level (%)
v	specific volume (m^3·kg^{-1})
V	compressor cubic capacity (cm^3)
$\dot{W}$	power input (W)
x	vapour quality
X	refrigerant concentration (%)

Greek Symbols

Δ	variation (increment or decrement)
ε	thermal effectiveness (%)
η	efficiency (%)

Subscripts

air	air
blend	it refers to the mixture
c	compressor
cal	calculated
CO_2	it refers to CO_2
crit	critical point
dis	discharge
env	environmental / ambient
ev	evaporator
exp	expansion
fin	final
G	geometric / global
gas	it refers to the additional fluid in the mixture
gc	gas-cooler
ihx	internal heat exchanger
in	inlet / initial
iso	isoentropic
k	condenser
liq	liquid
mix	it refers to the mixture
opt	optimum
out	out
prod	product
Pull-down	it refers to the pull-down test
sat	saturated
sf	secondary fluid
suc	suction port
V	volumetric
vap	vapour
w	it refers to weight
16 h	it refers to a 16 h energy consumption test

Table 1
Main properties of the analysed fluids.

Name	Family	Molar mass (g·mol^{-1})	NBP (°C)	P_{crit} (bar)	T_{crit} (°C)	Safety group	LFL (%)	UFL (%)	GWP$_{100}$ (AR5)
R-744	Inorganic	44.0	−78.4	73.8	31.1	A1	–	–	1
R-32	HFC	52.0	−51.7	57.8	78.1	A2L	13.3	29.3	677
R-41	HFC	34.0	−78.1	59.0	44.1	A2	7.1	19.9	116
R-152a	HFC	66.0	−24.0	45.2	113.2	A2	4.3	17.4	138
R-161	HFC	48.1	−37.5	50.5	102.1	A2	3.8	18.0	4
R-290	HC	44.1	−42.1	42.5	96.7	A3	2.0	10.0	3
R-1270	HC	42.1	−47.7	46.7	92.4	A3	2.2	11.0	2

method extends the subcritical operation of pure CO_2, minimizing the compressor work and the high throttling losses. Moreover, zeotropic glide allows a better matching between the refrigerant and the secondary fluid, reducing the irreversibility during the heat exchange process [21]. Another interesting point is the minimization of the triple-point of pure CO_2, which extends the operating range of CO_2 to temperatures below −56.6 °C depending on the refrigerant mixture [22,23].

During the last years, several authors have discussed using CO_2 mixtures as an alternative to pure CO_2 in vapour compression systems. Table 1 summarises most of these investigations, including the application, the character of the research (theoretical or experimental), the mixtures analysed and their optimum concentration (if reached). This table also included the operating conditions, the cycle characteristics and the most relevant conclusions from the analysis.

Author	Application	Character	Analysed mixture(s)	Operating conditions	Main cycle features	Conclusions
Di Nicola *et al.* [23]	Cascade	Theoretical	CO_2/R41 (50/50 %w) CO_2/R23 (40/60 %w) CO_2/R32 (50/50 %w) CO_2/R125 (27/73 %w)	T_k: 40 °C T_{ev}: −70 °C Optimization of the intermediate temperature	NH_3/CO_2 cascade cycle with IHX in the LT cycle.	The global COP with blends in the LT cycle is similar to that obtained using pure refrigerants.
Niu and Zhang [24]	Cascade	Experimental	CO_2/R290 (71/29 %m)	$T_{k\ in}$: no data $T_{ev\ in}$: −58 to −68 °C	R290/R13 cascade cycle with IHX in the LT cycle.	At −65 °C, the CO_2 blend performs better than R13 with higher COP (+34.2 %) and higher cooling capacity (+39.0 %).
Kim *et al.* [25]	Air Conditioning	Experimental	CO_2/R290 (75/25 %w)	$T_{k\ sf\ in}$: 30 / 36 °C $T_{ev\ sf\ in}$: 21 / 27 °C Mass charge optimization	Transcritical cycle with IHX.	AT the optimal charge, the COP rises 12.8 % and the cooling capacity decreases −22.7 %.
Onaka *et al.* [26]	Heat pump water heater	Theoretical	CO_2/RE170 (90/10 %w)	$T_{k\ sf\ in}$: 20 °C $T_{k\ sf\ out}$: 65 °C $T_{ev\ sf\ in}$: 20 °C $T_{ev\ sf\ out}$: 5 °C	Transcritical and subcritical cycle without IHX.	The COP of the cycle rises with the RE170 concentration. In transcritical operation, the maximum COP increment is 7.5 %.
Cox *et al.* [27]	Mobile air conditioning	Theoretical	CO_2/R41 (50/50 %m)	$T_{k\ sf\ in}$: 27 / 39 °C $T_{ev\ sf\ in}$: no data	Transcritical cycle without IHX.	At 27 °C the COP increases 17 % with regard to pure CO_2.
Sarkar and Bhattacharyya [28]	Heat pump for high temperature	Theoretical	CO_2/R600 (50/50 %w) CO_2/R600a (50/50 %w)	$T_{k\ sf\ in}$: 30 °C $T_{k\ sf\ out}$: 120 °C $T_{ev\ sf\ in}$: 30 °C $T_{ev\ sf\ out}$: 25 °C	Transcritical cycle with IHX.	Blends perform lower COP than pure CO_2 (-9.48 % and −1.76 %, respectively), but they work at lower discharge pressures (5.6 times lower).
Di Nicola *et al.* [29]	Cascade	Theoretical	CO_2/R170 (50/50 %w) CO_2/R290 (50/50 %w) CO_2/R1150 (50/50 %w) CO_2/R1270 (50/50 %w) CO_2/RE170 (50/50 %w)	T_k: 40 °C T_{ev}: −70 °C Optimization of the intermediate temperature	NH_3/CO_2 cascade cycle with IHX in the LT cycle	The global COP with blends in the LT cycle is lower to that obtained using pure refrigerants.
Fan *et al.* [30]	Heat pump water heater	Theoretical	CO_2/R290 (80/20 %w)	$T_{k\ sf\ in}$: 15 °C $T_{k\ sf\ out}$: 55 °C $T_{ev\ sf\ in}$: 20/15/10 °C $T_{ev\ sf\ out}$: 15/10/5°C	Transcritical cycle without IHX.	The COP and the heating capacity are increased up to 12.6 % and 34.2 %, respectively, regarding R22.
Dai *et al.* [31]	Heat pump water heater	Theoretical	10 different blends. The most relevant: CO_2/R41 (40/60 %w) CO_2/R32 (80/20 %w)	$T_{k\ sf\ in}$: 15 °C $T_{k\ sf\ out}$: 55 °C $T_{ev\ sf\ in}$: 15 °C $T_{ev\ sf\ out}$: 10 °C	Transcritical cycle without IHX.	COP increments of 4.03 % and 4.47 %, respectively
Jemni *et al.* [32]	Cascade	Theoretical	Different blends of CO_2 with R1270, R290, R170 and R600a as refrigerants in the LT and HT cycle.	$T_{k\ out}$: 40 °C $T_{ev\ out}$: −40 °C Optimization of the intermediate temperature	Cascade cycle without IHX	Pure CO_2 performs worse than mixtures in cascade and one-stage systems but lower than pure R22.
Bouteiller *et al.* [33]	Domestic water heater (DHW) and central heating (CH)	Experimental	CO_2/R290 (85/15 %m)	$T_{k\ sf\ in}$: 10 / 30 °C $T_{k\ sf\ out}$: 65 / 35 °C $T_{ev\ sf\ in}$: 7 °C	Transcritical cycle with IHX.	The blend reduces the performance of the cycle at the DHW conditions but increases the COP at the CH conditions.
Nasruddin *et al.* [34]	Cascade	Theoretical	CO_2/R170 (68/32 %w)	T_k: 56 °C T_{ev}: −49 °C Optimization of the intermediate temperature	Cascade cycle without IHX and R290 in the HT cycle.	Exergy and economic optimization to minimize both
Bouteiller *et al.* [35]	Heat pump water heater (DHW) and central heating (CH)	Experimental	CO_2/R1234yf (94.5/5.5 %m)	$T_{k\ sf\ in}$: 10 / 30 °C $T_{k\ sf\ out}$: 65 / 35 °C $T_{ev\ sf\ in}$: 7 °C	Transcritical cycle with IHX.	The blend reduces the performance of the cycle at the DHW conditions but increases the COP at the CH conditions.
Wang *et al.* [36]	Heat pump water heater and refrigerated cabinet	Theoretical	CO_2/R41 (50/50 %w)	$T_{k\ sf\ out}$: 35 to 50 °C T_{ev}: −10 to 5 °C Optimization of the intermediate temperature	Transcritical cycle with IHX.	The COP and the cooling capacity are enhanced up to 20.52 % and 25.67 %, respectively, with the blend.
Tobaly *et al.* [37]	Air Conditioning and refrigeration	Experimental	CO_2/R290 The optimum composition depends on the operating conditions	$T_{k\ sf\ in}$: 35 / 40 °C $T_{ev\ sf\ in}$: 12 to −5°C $T_{ev\ sf\ out}$: 7 to −10 °C	Transcritical cycle with IHX.	The COP is enhanced up to 19.7 % but the cooling capacity decreases up to 18 %.
Yu *et al.* [38]	Mobile air conditioning (cooling)	Experimental	CO_2/R290 with different R290 mass fractions from 0 to 50 %	$T_{k\ sf\ in}$: 27 to 40 °C $T_{ev\ sf\ in}$: 27 / 40 °C Mass charge and compressor rotation speed optimization	Transcritical cycle with IHX.	At fixed cooling capacity, the mass fraction of 30/70 %w optimizes the COP from 22.1 % to 18.4 % depending on $T_{k\ sf\ in}$.
Ju *et al.* [39]	Heat pump water heater	Experimental	CO_2/R290 (88/12 %w)	$T_{k\ sf\ in}$: 15 °C $T_{k\ sf\ out}$: 55 °C $T_{ev\ sf\ in}$: 20 °C $T_{ev\ sf\ out}$: 15 °C	Transcritical cycle without IHX.	The COP and the heating capacity are increased up to 11 % and 17.5 %, respectively, regarding R22.

(continued)

Author	Application	Character	Analysed mixture(s)	Operating conditions	Main cycle features	Conclusions
Yu *et al.* [40]	Mobile air conditioning (cooling and heating)	Experimental	CO_2/R41 with different R41 mass fractions from 0 to 100 %	$T_{k\ sf\ in}$ and $T_{ev\ sf\ in}$: -10/-20/27/40 °C Mass charge and compressor rotation speed optimization	Transcritical cycle with IHX.	The COP in the heating mode can be improved up to 14.5 %. In Cooling mode the COP has a maximum improvement of 25.7 %.
Kumar and Kumar [41]	Refrigeration	Theoretical	CO_2/R290 (15/85 %w)	T_k: 35 to 45 °C T_{ev}: -7 to 12 °C	Transcritical cycle with IHX.	The COP of the mixture is similar than pure CO_2 but with higher critical temperature and lower critical pressure.
Massuchetto *et al.* [42]	Cascade	Theoretical	Different blends of CO_2 with R1270, RE170 and R717. The most relevant: CO_2/RE170 (20/80 %w) in the HT cycle and (10/90 %w) in the LT cycle	$T_{k\ sf\ in}$: 25 °C $T_{k\ sf\ out}$: 50 °C $T_{ev\ sf\ in}$: -5 °C $T_{ev\ sf\ out}$: -20 °C Optimization of the CO_2 mass composition	Cascade cycle without IHX in the LT cycle.	The global COP of the cascade system using the CO_2/RE170 mixture is up to 31 % higher than this system operating with pure refrigerants.
Sun *et al.* [43]	Heat pump water for heating and cooling	Experimental	CO_2/R32 at different mass fractions from 0 to 50 % of R32	$T_{k\ sf\ in}$: 20/40 °C $T_{k\ sf\ out}$: 45/55 °C $T_{ev\ sf\ in}$: 12 °C $T_{ev\ sf\ out}$: 7 °C Optimization of the CO_2 mass composition	Transcritical cycle with IHX.	The COP for heating and cooling increases with the mass fraction of R32. However, the heating and cooling capacity diminishes.
Sánchez *et al.* [44]	Refrigeration	Experimental	CO_2/R1270 (91/9%w)	$T_{k\ sf\ in}$: 25 °C $T_{ev\ sf\ in}$: ~1 °C	Transcritical cycle with IHX.	The use of the CO_2/R1270 blend instead of pure CO_2 reduces the energy consumption of a beverage cooler 10.3 %.
Sobieraj [45]	Cascade	Experimental	CO_2/R290 (67/33 %w) CO_2/R32 (67/33 %w)	$T_{ev\ in}$: -72.3 to -71.0 °C $T_{ev\ out}$: -71.0 to -64.8 °C	Cascade cycle with IHX in the LT cycle.	The system reaches evaporating temperatures below -55 °C
Xie *et al.* [46]	Refrigeration	Theoretical	CO_2/R152a (82.5/17.5 %w) CO_2/R161 (85/15 %w)	$T_{gc\ out}$: 35 °C T_{ev}: 15 °C	Transcritical cycle without IHX.	The COP increases 30.1 % with the blend CO_2/R152a and 32.5 % with CO_2/R161

From the summary of Table 1, it can be affirmed that using zeotropic or near-azeotropic mixtures with CO_2 is a feasible solution that minimizes the complexity of the transcritical cycle, enhances the COP and reduces the working pressures of the plant [47]. However, CO_2 mixtures generally provide lower heating/cooling capacity, affecting the
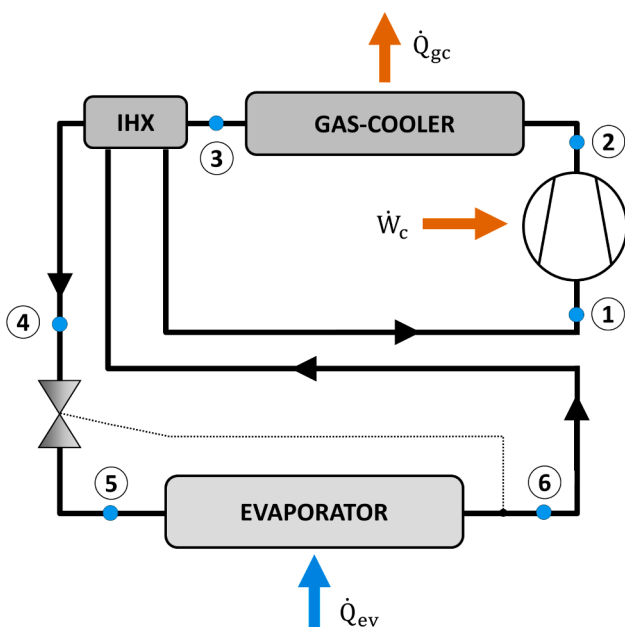

Fig. 1. Schematic diagram of the single-stage vapour compression system.

compressor's dimensions or operation. Moreover, they operate with lower boiling heat transfer, expecting a higher heat transfer area than pure CO_2 [48]. Therefore, it does not seem easy to predict the positive effect of mixtures if they are used as a *drop-in* in a current transcritical cycle where the flammability risk is relevant.

Accordingly, this work explores the benefits of using different CO_2 binary blends as *drop-ins* of pure CO_2 in a vertical display cabinet. The assessment starts with a theoretical analysis, selecting the most relevant zeotropic blends attempting to the criterion of GWP below 150, non-flammability conditions, increment of COP regarding pure CO_2, and high availability of the components. Later, the selected CO_2-based blends are developed and energetically tested in a vertical display cabinet under two ambient conditions while maintaining a desired product target temperature. The positive results reported by the blends of CO_2/R1270 and CO_2/R32 demonstrate the possibility of introducing alternative fluids as *drop-ins* of pure CO_2, providing better performance and energy savings.

2. Theoretical analysis

2.1. Cycle description

The refrigerating cycle used to determine the CO_2 mixtures analysed in this work consists of a single-stage vapour compression cycle with an internal heat exchanger (IHX), as is depicted in Fig. 1. This cycle is typically used in small-capacity systems such as bottle coolers or merchandiser systems with a unique expansion device [49]. It works in transcritical or subcritical conditions depending on the critical temperature of the mixture and the heat rejection temperature (ambient temperature).

Table 2
Non-flammable CO_2-based mixtures.

Mixture	FIP [1]	% CO_2 (in mass)	% Flammable Gas (in mass)	GWP_{100} (AR5)	P_{crit} (bar)	T_{crit} (°C)	Total Glide (K) (-10 °C, x = 0.5)
CO_2 + R32 [2]	0.602	56.1 %	43.9 %	297.6	754.52	54.47	13.40
CO_2 + R32	0.602	78.0 %	22.0 %	149.7	75.81	43.24	6.49
CO_2 + R41	0.751	79.6 %	20.4 %	24.5	71.54	34.50	1.12
CO_2 + R152a	0.854	79.5 %	20.5 %	138.0	81.39	51.88	23.72
CO_2 + R161	0.878	86.9 %	13.1 %	1.4	79.37	46.41	12.41
CO_2 + R290	0.922	92.2 %	7.8 %	1.2	69.80	31.68	2.20
CO_2 + R1270	0.921	92.4 %	7.6 %	1.1	76.17	36.95	3.37

[1] concentration in mol of CO_2, in the mixture of flammable gas and CO_2.
[2] mixture exceeds the maximum GWP allowed (150).

Table 3
Input data to the computation model.

Variable	Description	Value
T_{env}	Ambient temperature	30 °C
ΔT_{env}	Approach temperature in the condenser/gas-cooler	2.3 K
V_G	Compressor cubic capacity	1.1 cm³
N	Compressor rotation speed	2900 rpm
ε_{ihx}	IHX thermal effectiveness	68.9 %
$SH_{suc}(K)$	Non-useful superheating	2 K
$T_{air\ in}$	Air inlet temperature (evaporator)	1.9 °C
$T_{air\ out}$	Air outlet temperature (evaporator)	−1.6 °C
$SH_{ev}(K)$	Useful superheating	4.2 K
LMTD	Logarithmic mean temperature	7.9 K

2.2. Fluid selection criteria

The developed blends are binary mixtures of CO_2 and a secondary fluid which main properties are summarized in Table 1 including thermophysical properties, safety data and environmental impact.

The thermophysical properties selected to identify the fluids are molar mass, normal boiling point (NBP), critical pressure (P_{crit}), and critical temperature (T_{crit}). All are determined with the database of RefProp® v.10.0. Safety group is determined with the ASHRAE Standard 34 [50], while low and upper flammability limits (LFL, UPL) are extracted from the work of Calm [51]. Finally, the environmental impact of global warming potential (GWP) is taken from the IPCC Fifth Assessment Report [52].

As the main objective is finding potential CO_2 *drop-ins*, it is mandatory achieving the advantages reported by CO_2 in terms of non-flammability and low-GWP according to the limits proposed by the EU regulation n° 514/2014. Therefore, the first step consists of selecting the maximum quantity of additional fluid that can be added to CO_2 maintaining both: non-flammability and GWP ≤ 150.

For the flammability analysis is important to notice that all fluids selected to mix with CO_2 are flammable, and their flammability range are determined by the upper and the lower flammability limits. This flammability range, defined as the volume concentration of the flammable gas in the dry air-gas mixture, can be reduced by adding an inert gas such as pure CO_2 [53]. The inert gas minimizes the flammability range until the two limits coincide at a single point called Fuel Inertization Point (FIP). The FIP defines the maximum concentration of flammable gas in the dry air - gas - CO_2 mixture that never generates a flammable mixture regardless of the amount of air added or removed from the mixture. Therefore, it fixes the maximum concentration of the flammable gas that can be added to CO_2 maintaining non-flammable conditions. From the equations adjusted by Kondo *et al.* [54] to determine the values of UFL and LFL limits depending on the flammable gas and the amount of CO_2 added, it is possible to determine the FIP which results are summarized in Table 2. Moreover, the critical point, and the total glide at −10 °C and a vapour quality (x) of 50 % are also included using the mixing rules programmed in the RefProp® software.

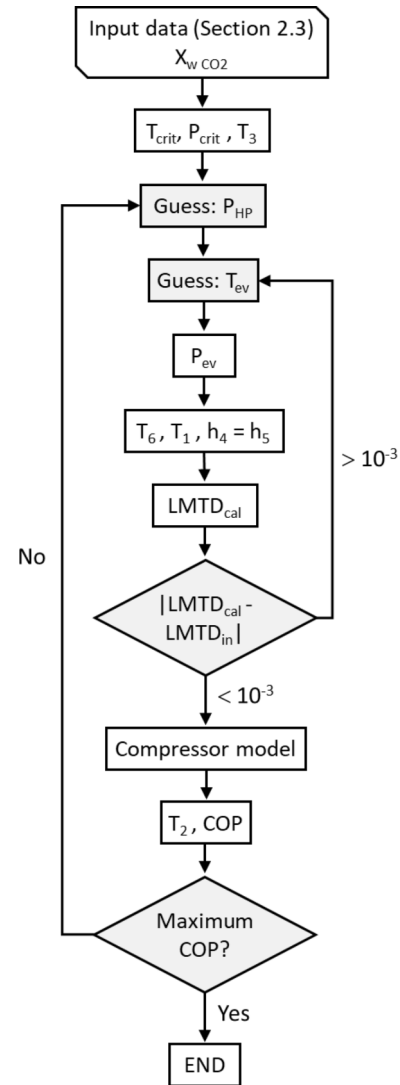Eq. (1) defines the GWP of the mixture by taking into account the

Fig. 2. Computational model flowchart.

Table 4
Experimental coefficients for the CO_2 hermetic compressor.

Coefficient	η_V	η_G
a_0	0.8748614461	0.5228303246
a_1	0.0046715654	−0.0001637017
a_2	−0.0035665060	−0.0002120453
a_3	0.0022098618	0.0017040840
ε_{max}	6.50 %	7.30 %

GWP of each fluid and its mass fraction expressed as a decimal. Assuming a GWP limitation of 150, Eq. (2) determines the maximum flammable gas mass fraction limiting the *R32* mass concentration shown in Table 2.

$$GWP_{mix} = X_{w\,CO2} \cdot GWP_{CO2} + X_{w\,gas} \cdot GWP_{gas} \tag{1}$$

$$\frac{150 - X_{w\,CO2} \cdot GWP_{CO2}}{GWP_{gas}} > X_{w\,gas} \tag{2}$$

2.3. Model input data

The operating conditions used in the computational model have been extracted from the test campaign by Sánchez *et al.* [55] using pure CO_2 in a vertical beverage cooler. These values were obtained by averaging the registered data during the compressor operation, excluding the compressor starting. The information gathered in Table 3 includes the heat rejection temperature (T_{env}), the approach temperature at the exit of the gas-cooler (or condenser) (ΔT_{env}), the compressor cubic capacity (V_G), the compressor rotation speed (N), the IHX thermal effectiveness (ε_{IHX}) and the non-useful superheating at the suction pipeline (SH_{suc}). Moreover, due to the zeotropic behaviour of the CO_2-based mixtures, the evaporator has been modelled with the air temperature at the inlet and outlet of the evaporator ($T_{air\,in}$, $T_{air\,out}$), the useful superheating (SH_{ev}) and its logarithmic mean temperature (LMTD). As a first approach, the input data are similar for all CO_2-based mixtures. However, a series of experimental tests are required to corroborate the theoretical results as will be presented in Section 4.

2.4. Mathematical model

The cycle described in Fig. 1 was evaluated with a computational model based on the principles of mass and energy conservation. The model was developed with MatLab® R2016a using the thermophysical properties of RefProp® v.10.0, which contains the mixing rules and the binary mixing coefficients for all mixtures analysed in this work.

The flowchart calculation of the computational model is depicted in Fig. 2, using as input data the data summarized in Table 3, the selected CO_2 binary mixture, and the CO_2 mass fraction ($X_{w\,CO2}$).

According to Fig. 2, the model determines the critical point (T_{crit} and P_{crit}) using the chosen mixture and the CO_2 mass fraction ($X_{w\,CO2}$). Then, the temperature of state point 3 (T_3) is claculated with Eq. (3) using the ambient temperature (T_{env}) and the approach temperature in the gas-cooler / condenser (ΔT_{env}).

$$T_3 = T_{env} + \Delta T_{env} \tag{3}$$

Once T_3 is obtained, the computational model has an iterative calculation loop for determining the heat rejection pressure (P_{HP}) that

Fig. 3. Effect of refrigerant mass fraction on the ΔCOP.

maximises the COP. This iterative loop needs a heat rejection pressure range that is defined by comparing T_{crit} and T_3. Thus, if T_3 is lower than T_{crit}, condensation is possible (subcritical operation), so the minimum value of P_{HP} is the condensation pressure at T_3, and the maximum corresponds to the critical pressure (P_{crit}). If not, a transcritical operation is possible, so the maximum pressure is fixed to 100 bar, and the minimum value is P_{crit}. The range defined allows an iterative loop calculating the refrigerating cycle from the minimum heat rejection pressure to the maximum value with increments of 0.005 bar. Whatever the conditions, the model considers no pressure drop inside the pipelines and heat exchangers.

Similar to P_{HP}, the model assumes an initial value for the evaporating temperature (T_{ev}) at saturated vapour conditions. Temperature T_6 is calculated by adding the useful superheating (SH_{ev}) to T_{ev} (Eq. (4)), while T_1 and h_4 are obtained with an energy analysis in the IHX (Eq. (5), (6)). Since isenthalpic expansion process is assumed in the expansion valve, enthalpy h_4 is equal to h_5.

$$T_6 = T_{ev} + SH_{ev} \tag{4}$$

$$T_1 = T_6 + \varepsilon_{ihx} \cdot (T_3 - T_6) \tag{5}$$

$$h_5 = h_4 = h_3 - (h_1 - h_6) \tag{6}$$

Taking into account the non-azeotropic conditions of the mixture, the logarithmic mean temperature difference in the evaporator ($LMTD_{cal}$) is calculated with Eq. (7), neglecting the SH_{ev}. Temperature T_5 is determined with the pressure at the saturated vapour conditions of T_{ev} and h_5.

$$LMTD_{cal} = \frac{(T_{air\,in} - T_6) - (T_{air\,out} - T_5)}{\ln\left(\frac{T_{air\,in} - T_6}{T_{air\,out} - T_5}\right)} \tag{7}$$

According to Fig. 2, the result from Eq. (7) is compared to the initial value from Table 3 for an iterative process. This iteration loop allows determining the evaporation pressure (P_{ev}) as input data to the semi-empirical compressor model proposed by Sánchez *et al.* [56] (Eq. (8), (9), Table 4). Although this model is adjusted using CO_2 as refrigerant, we assumed it is also valid for all CO_2-based mixtures since no compressor models have been published in literature with these analysed mixtures.

Finally, temperature at the suction port (T_{suc}) is defined through Eq. (10) by adding the non-useful superheating (SH_{suc}) to temperature T_1.

$$\eta_V = a_0 + a_1 \cdot P_{ev} + a_2 \cdot P_{HP} + a_3 \cdot T_{suc} \tag{8}$$

$$\eta_G = b_0 + b_1 \cdot P_{ev} + b_2 \cdot P_{HP} + b_3 \cdot T_{suc} \tag{9}$$

$$T_{suc} = T_1 + SH_{suc} \tag{10}$$

Outputs from the compressor model are volumetric (η_V) and global efficiency (η_G), which allows for calculating the refrigerant mass flow rate ($\dot{m}$) and the compressor power consumption ($\dot{W}_C$), using the specific volume at the suction port (v_{suc}) and the isentropic compression work ($h_{2\,iso} - h_{suc}$) (Eq. (11), (12)).

$$\dot{m} = \frac{\eta_V \cdot V_G \cdot N/60}{v_{suc}} \tag{11}$$

$$\dot{W}_c = \dot{m} \cdot \frac{(h_{2\,iso} - h_{suc})}{\eta_G} \tag{12}$$

Finally, the cooling capacity ($\dot{Q}_{ev}$) and the coefficient of performance (COP) of the refrigerating cycle are obtained by Eq, (13) and (14).

$$\dot{Q}_{ev} = \dot{m} \cdot (h_6 - h_5) \tag{13}$$

$$COP = \frac{\dot{Q}_{ev}}{\dot{W}_c} \tag{14}$$

Table 5
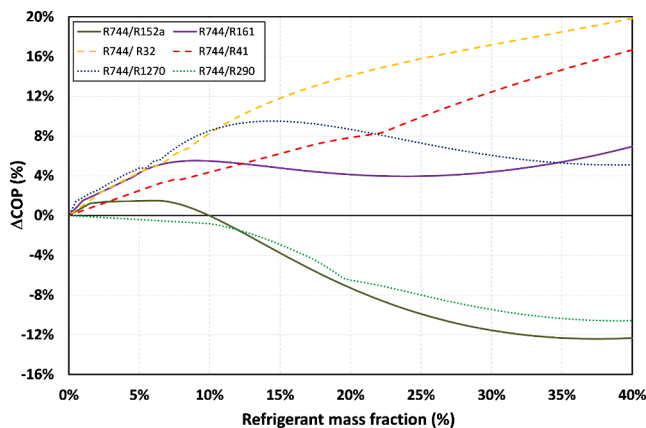Optimal results for pure CO_2 and CO_2-based mixtures.

Mixture	Optimum mass fraction (%)	P_{crit} (bar)	T_{crit} (°C)	T_{ev} (°C)	P_{HP} (bar)	$\dot{W}_c$ (W)	$\dot{Q}_{ev}$ (W)	COP	$\Delta \dot{W}_c$ (%)	$\Delta \dot{Q}_{ev}$ (%)	ΔCOP (%)	GWP_{100} (AR5)	Total Glide (K) (-10 °C, x = 0.5)
Pure CO_2	100 / 0	73.77	30.98	−7.86	80.50	248.85	421.31	1.693	–	–	–	1.0	0.0
CO_2 + R32	78 / 22	75.82	43.24	−7.86	62.01	194.09	377.27	1.944	−22.0	−10.5	14.8	149.7	8.41
CO_2 + R41	79.5 / 20.5	71.53	34.52	−7.81	71.53	223.28	408.07	1.828	−10.3	−3.1	7.9	24.6	1.12
CO_2 + R152a	94 / 6	77.28	37.55	−7.92	70.49	217.93	374.51	1.718	−12.4	−11.1	1.5	9.2	8.44
CO_2 + R161	91 / 9	70.25	36.88	−8.17	66.37	204.36	365.05	1.786	−17.9	−13.4	5.5	1.3	11.18
CO_2 + R1270	92.5 / 7.5	76.15	36.88	−7.74	69.98	217.80	393.52	1.807	−12.5	−6.6	6.7	1.1	3.31
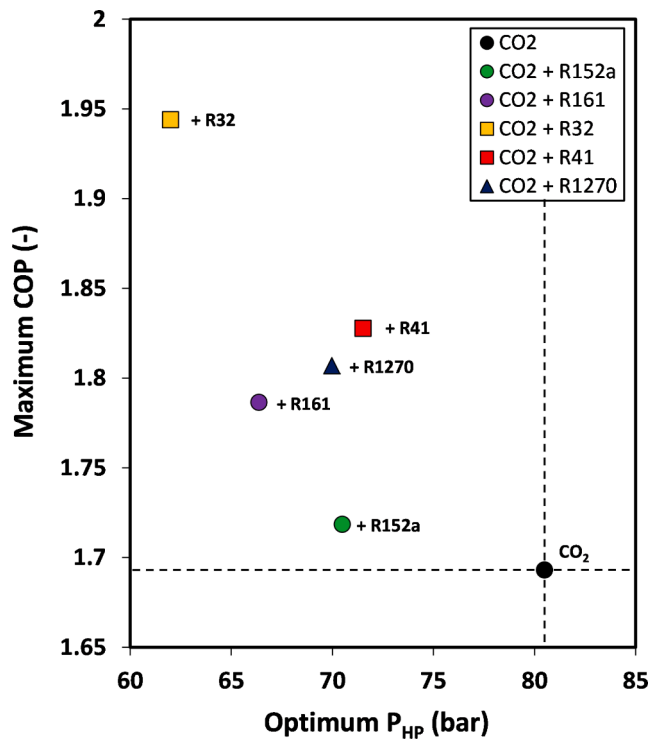
Fig. 4. Maximum COP and optimal pressure for the CO_2-based mixtures analysed.

Fig. 5. Cooling capacity and compressor power consumption at the optimal operating conditions.

To determine the maximum COP, the computational model repeats the calculation process described above at different heat rejection pressures obtaining a data-matrix, where the maximum COP is obtained. This sequence is repeated for different CO_2 mass fractions with increments of 0.5 % resulting in the Figures presented in Section 2.5 at the optimum heat rejection pressures.

2.5. Model results

Taking pure CO_2 as reference, the COP variation (ΔCOP) is calculated with Eq. (15) at the optimal operating conditions since it is the desired operating point for a refrigerating plant.

$$\Delta COP = \frac{(COP_{blend} - COP_{CO2})}{COP_{CO2}} \qquad (15)$$

Fig. 3 shows how the refrigerant mass fraction affects the ΔCOP for all the CO_2-based mixtures summarized in Table 2. As the mass fraction is limited in all cases, Fig. 3 shows a maximum of 40 %.

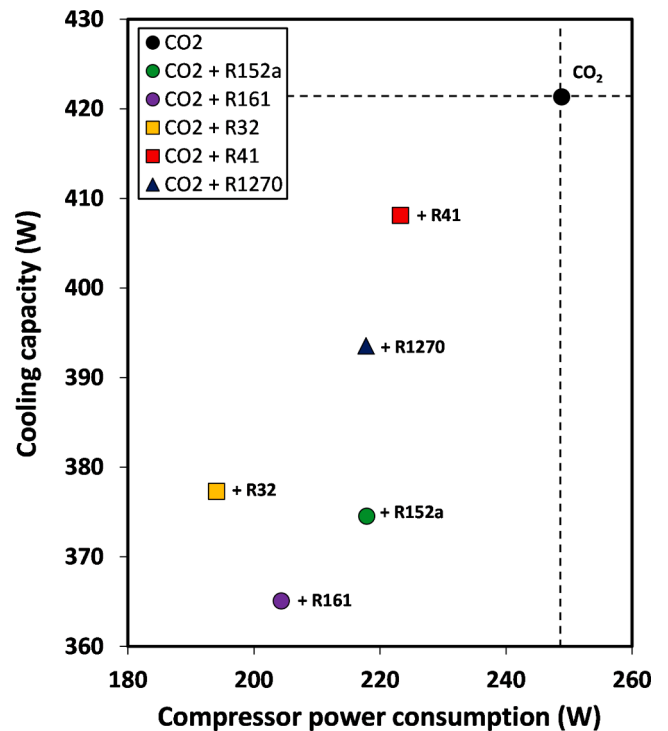According to Fig. 3, for each binary mixture, there is a refrigerant mass fraction that maximises the COP except for R290, where the model does not predict any COP improvement under the working conditions described in Section 2.3. However, it is important to note that optimum mass fractions must be lower than the values reported in Table 2 according to the requirements of low-GWP and non-flammability. Therefore, Table 5 summarises the optimal mass fractions for each binary mixture, including the values of the critical point, evaporating temperature, optimal heat rejection pressure (P_{opt}), compressor power consumption, cooling capacity, COP, ΔCOP and GWP. For a better view, Fig. 4 presents the mixture's COP with their corresponding optimal heat rejection pressure, and Fig. 5 shows the cooling capacity and the compressor power consumption.

The results from Table 5 reveal that all mixtures increase the critical temperature of pure CO_2 while some reduce the critical pressure. Nevertheless, all blends reduce the optimal pressure from 9.0 to 18.5 bar concerning pure CO_2, which minimises the compressor's power consumption from 10.3 to 22.0 % (Figs. 4 and 5). The main consequence of this positive effect is the enhancement of COP up to 14.8 % for R32, followed by R41 (7.9 %), R1270 (6.7 %), R161 (5.5 %), and R152a (1.5 %) (Fig. 4). Both positive effects are in concordance with the results presented in the literature, as well as the depletion of cooling capacity
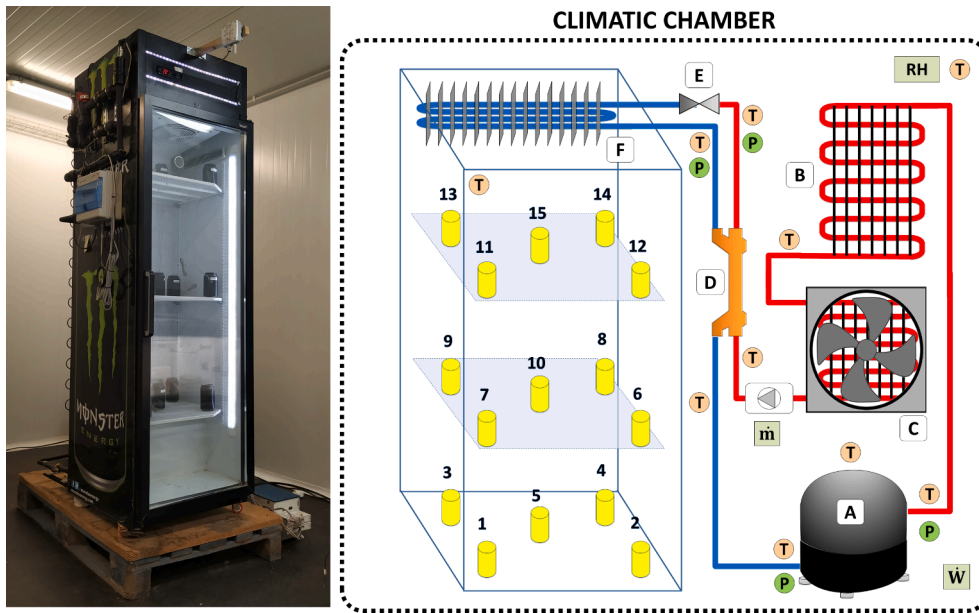
Fig. 6. Vertical display cabinet (left) and its schematic diagram (right).

Table 6
Main characteristics of the refrigerating components.

ID	Description	Main characteristics
(A)	Compressor	Hermetic compressor. Capacity 1.1 cm^3. Nominal rotation speed: 2900 rpm (50 Hz)
(B)	Condenser	Wire-on-tube heat-exchanger. Natural convection. Inner heat transfer area: 0.186 m^2
(C)	Condenser	Finned-tube heat-exchanger. Forced convection. Inner heat transfer area: 0.089 m^2
(D)	IHX	Concentric tube heat-exchanger. Inner heat transfer area: 0.01 m^2
(E)	Thermostatic Valve	Electronic expansion valve controlling the superheating degree at the evaporator (6 K)
(F)	Evaporator	Finned-tube heat-exchanger. Forced convection. Inner heat transfer area: 0.186 m^2

Table 7
Main characteristics of the measurement elements.

Number	Measured Variable (symbol)	Measurement device	Range	Uncertainty
10	Temperature (T)	T-type thermocouple	−40 to 125 °C	± 0.5 K
15	Product temperature	T-type thermocouple	−40 to 125 °C	± 0.5 K
2	Pressure (high-pressure) (P)	Pressure transducer	0 to 160 bar	± 0.5 % of the spam
2	Pressure (low-pressure) (P)	Pressure transducer	0 to 60 bar	± 0.5 % of the spam
1	Refrigerant mass flow rate ($\dot{m}$)	Coriolis mass flow meter	0 to 50 kg·h^{-1}	± 0.5 % of reading
1	Electric power consumption ($\dot{W}$)	Wattmeter	0 to 1000 W	± 0.5 % of reading
1	Relative humidity (RH)	Hygrometer	5 to 98 %	± 2 %

shown in Fig. 5. This last must be considered if a simple *drop-in* process is carried out because the cooling capacity depreciation will increase the compressor's running time. Accordingly, the second part of this manuscript is focused on energy tests to assess the appropriateness of the CO$_2$-based mixtures in terms of energy savings.

3. Experimental approach

To demonstrate the proper operation of the blends described in the previous section, a series of energy tests were performed in a transcritical refrigerating cycle installed in a display cooler. The mixtures used are CO$_2$/R32 and CO$_2$/R1270 due to the positive results presented above and their high availability in the market: R32 is widely used in air conditioning [57], and R1270 is proposed as an alternative to R290 [58]. This section describes the refrigerating setup and the experimental methodology followed during tests.

3.1. Refrigeration facility

The experimental facility consists of a vertical display cabinet with a glass door and dimensions of 620 (L) × 2000 (H) × 655 (D) mm, as shown in Fig. 6 (left). The display is equipped with a single-stage vapour compression system whose main elements are depicted in Fig. 6 (right), and their main characteristics are gathered in Table 6. The finned-tube heat exchangers have two axial fans to force the air through them, which power consumption is included in the energy consumption tests.

Excepting the discharge line, all the pipelines were insulated with a low-thermal conductivity foam to reduce the heat transfer to the environment.

To manage the inner temperature, the cabinet includes a temperature controller that switches off the refrigeration system, including axial fans, when the internal temperature reaches the desired set-point. Similarly, the controller switch on the compressor and the fans when the inner temperature is 3 K higher than the set-point. The defrosting process is applied every 8 h, stopping the refrigeration unit and waiting for a temperature of 5 °C at the evaporator surface.

According to Fig. 6, the system contains a series of measurement elements to evaluate the operation of the refrigeration facility. Table 7 summarizes the main information of these elements, including the number, measurement range and uncertainty.

The wattmeter is installed at the power supply input of the display cabinet to measure the global power consumption, including the refrigeration cycle, fans, lights, and the temperature controller. The product temperature is measured with 15 test cans distributed equally at three heights, as Fig. 6 shows, containing a mixture of water and propylene-glycol (67/33 % by volume) and an immersion T-thermocouple.
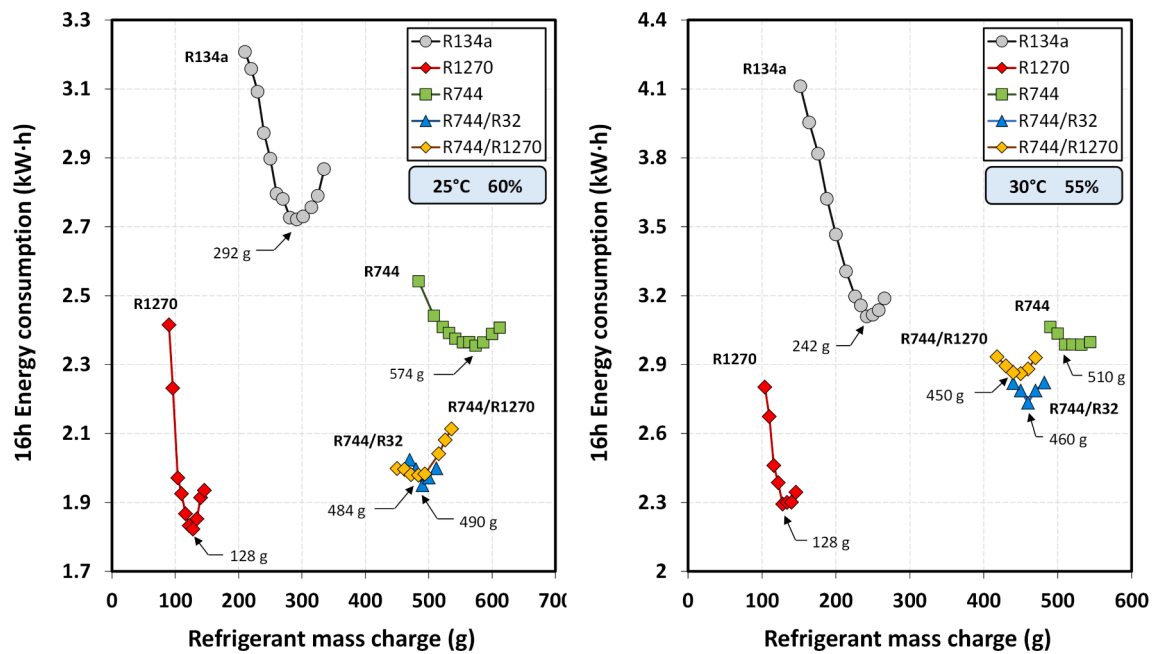
Fig. 7. Refrigerant mass charge optimization at Class III (left) and Class IV (right) conditions.
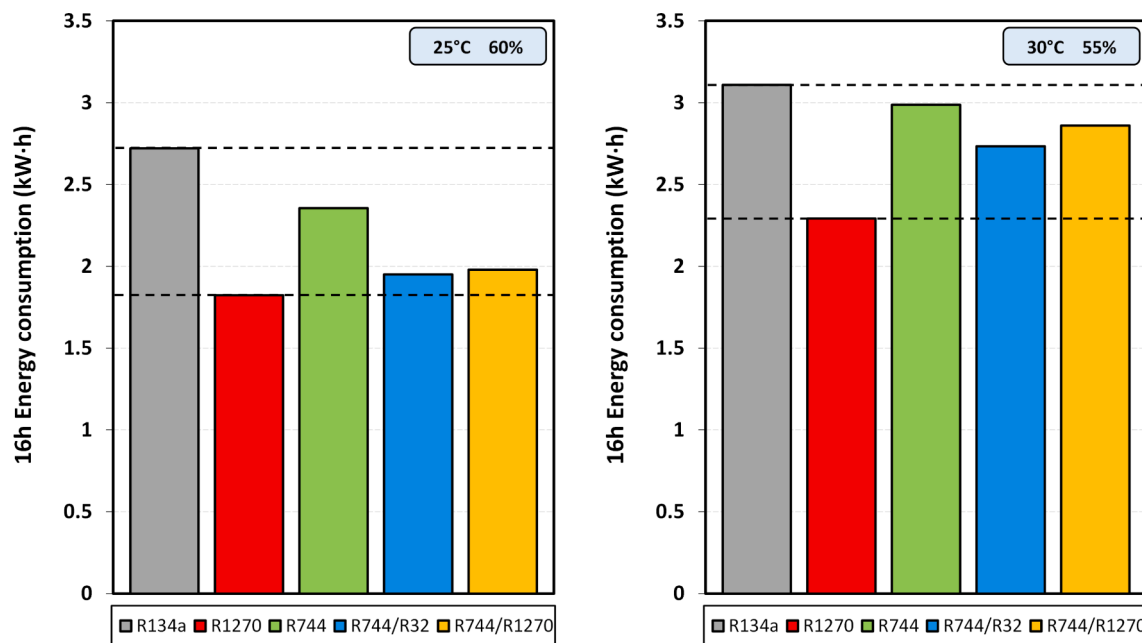

Fig. 8. Optimal energy consumption at Class III (left) and Class IV (right) conditions.

All data from measuring devices are gathered by a National Instruments® SCXI-1000 DAQ-system every 5 s and stored in a personal computer. The subsequent data processing is performed with the software MatLab® and the libraries of RefProp®.

3.2. Tested refrigerants

The refrigerant blends selected for the experimental analysis were $CO_2/R32$ (78.0/22.0 % in mass) and $CO_2/R1270$ (92.5/7.5 % in mass). Moreover, the setup was previously tested with pure CO_2, R134a and R1270 maintaining the same operating conditions but changing the compressor and the pressure transducers from Table 7. More information about these tests can be found in Sánchez et al. [55].

To manufacture the CO_2 blends, a vessel of 5 litters was used to mix the pure fluids at the tested ambient conditions described in Section 3.3. The mass introduced was weighed using a precision scale with an uncertainty of ± 1 g. To ensure a uniform mixture of fluids, the blend was maintained always in vapour phase by limiting the mass of the blend below the maximum defined by the density of the blend at vapour saturation conditions and the vessel volume. Moreover, a heating resistor was used to warm up the vessel ensuring vapour phase during the mass charge of the refrigerating plant.

3.3. Test conditions and experimental procedure

The experimental tests performed to analyse alternative blends of

Table 8
Main parameters of the refrigerating unit at the optimal mass charge.

Refrigerant	m_{opt} (g)	T_{env} (°C)	RH_{env} (%)	T_{prod} (°C)	T_{ev} (°C)	T_k (°C)	T_{dis} (°C)	P_{dis} (bar)	P_{suc} (bar)	Pressure ratio (P_{dis}/P_{suc})	$D_{cyle\ ON}$ (%)	$\dot{W}_c$ (W)	E_{16h} (kW·h)
Class III (25 °C; 60 %)													
CO_2 / R32	490	24.9	59.9	3.1	−8.6	36.7	65.7	64.2	20.2	3.2	37.3	295.1	1.95
	± 1	± 0.3	± 2.3	± 0.2	± 1.0	± 0.9	± 2.2	± 1.3	± 0.9	± 0.2		± 2.7	
CO_2 / R1270	484	24.9	59.7	3.1	−10.0	35.1	65.0	73.3	23.2	3.2	36.0	314.6	1.98
	± 1	± 0.3	± 2.6	± 0.3	± 0.8	± 0.7	± 1.9	± 1.4	± 0.9	± 0.2		± 4.2	
CO_2	574	24.7	58.5	3.1	−8.4	27.0 (*)	59.0	78.8	27.7	3.0	40.8	343.0	2.35
	± 1	± 0.3	± 2.8	± 0.2	± 1.1	± 1.0	± 2.0	± 1.7	± 0.9	± 0.2		± 6.2	
R134a	292	25.0	59.6	3.1	−9.4	32.8	69.5	8.9	1.9	4.7	53.1	297.7	2.72
	± 1	± 0.1	± 1.5	± 0.3	± 0.4	± 0.2	± 0.4	± 0.1	± 0.1	± 0.0		± 2.2	
R1270	128	24.5	58.8	3.1	−11.2	32.3	55.9	14.1	4.1	3.5	37.6	267.4	1.82
	± 1	± 0.3	± 3.3	± 0.2	± 0.3	± 0.5	± 0.8	± 0.1	± 0.1	± 0.0		± 1.7	
Class IV (30 °C; 55 %)													
CO_2 / R32	460	30.3	54.1	3.2	−8.8	40,3	80.2	71.2	20.1	3.6	53.1	307.0	2.73
	± 1	± 0.5	± 3.6	± 0.3	± 0.7	± 0.6	± 1.0	± 1.0	± 0.4	± 0.1		± 2.0	
CO_2 / R1270	450	30.3	53.8	3.2	−9.1	31.6 (*)	77.7	79.0	23.9	3.3	53.5	321.8	2.86
	± 1	± 0.5	± 3.5	± 0.2	± 1.0	± 0.8	± 1.9	± 1.6	± 0.6	± 0.1		± 4.0	
CO_2	510	30.1	53.8	3.2	−7.8	31.9 (*)	77.2	80.6	28.2	2.9	55.8	337.7	2.99
	± 1	± 0.5	± 3.7	± 0.4	± 0.8	± 0.9	± 2.7	± 1.3	± 0.7	± 0.1		± 3.5	
R134a	242	29.8	54.5	3.1	−10.0	37.4	72.3	10.0	1.9	5.3	59.1	311.8	3.11
	± 1	± 0.3	± 2.5	± 0.3	± 0.5	± 0.7	± 0.6	± 0.2	± 0.1	± 0.1		± 3.0	
R1270	138	30.1	55.1	3.2	−11.3	37.0	66.5	15.7	4.1	3.9	47.8	277.4	2.29
	± 1	± 0.3	± 1.2	± 0.3	± 1.0	± 0.3	± 1.1	± 0.1	± 0.2	± 0.2		± 3.4	

(*) In transcritical conditions it refers to the gas-cooler exit temperature.
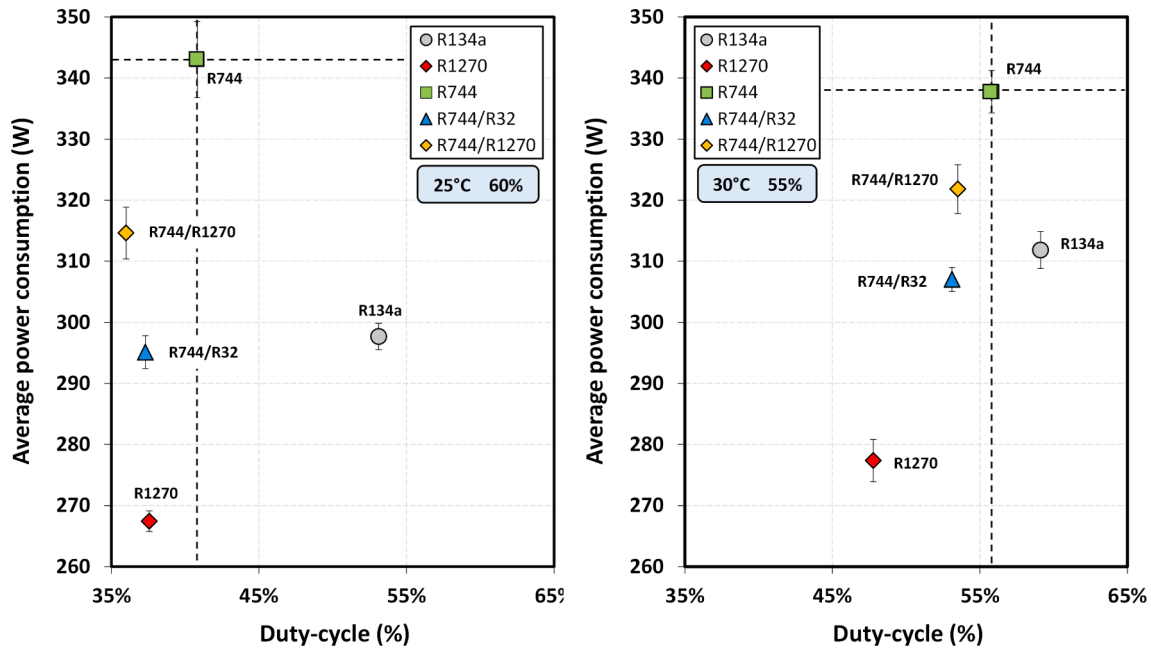

Fig. 9. Display power consumption vs duty-cycle at Class III (left) and Class IV (right) conditions.

CO_2 are based on the energy consumption of the whole display cabinet under similar operating conditions during a specific time. These tests allow for optimising the refrigerant mass charge that minimises the energy consumption and determining the time and energy invested by the refrigerating system to cool down the product from ambient conditions to the desired set point temperature. For easy understanding, the first tests are usually known as "energy consumption tests", while the second is "pull-down tests".

The operating conditions of the display cabinet were fixed by the average product temperature, and the ambient conditions (temperature and relative humidity). All tests were performed in a climatic chamber at two different ambient conditions according to ISO 23953–2: class III (25

°C; 60 %) and class IV (30 °C; 55 %). The average product temperature was maintained around 3 °C with a maximum temperature of 7.2 °C and a minimum above 0 °C [49]. The set-point was varied during tests from 0.9 to 1.1 °C to reach the desired average product temperature.

Regarding the experimental procedure, energy consumption tests were performed first to determine the optimum refrigerant mass charge. Then, pull-down tests were carried on with this optimal mass charge. The test order used in the campaign was: pure CO_2, CO_2/R32 and CO_2/R1270. The reference refrigerants R1270 and R134a were tested previously. In each case, the electronic expansion valve was upgraded, and the refrigerant facility was empty using a vacuum pump working for at least 40 min.
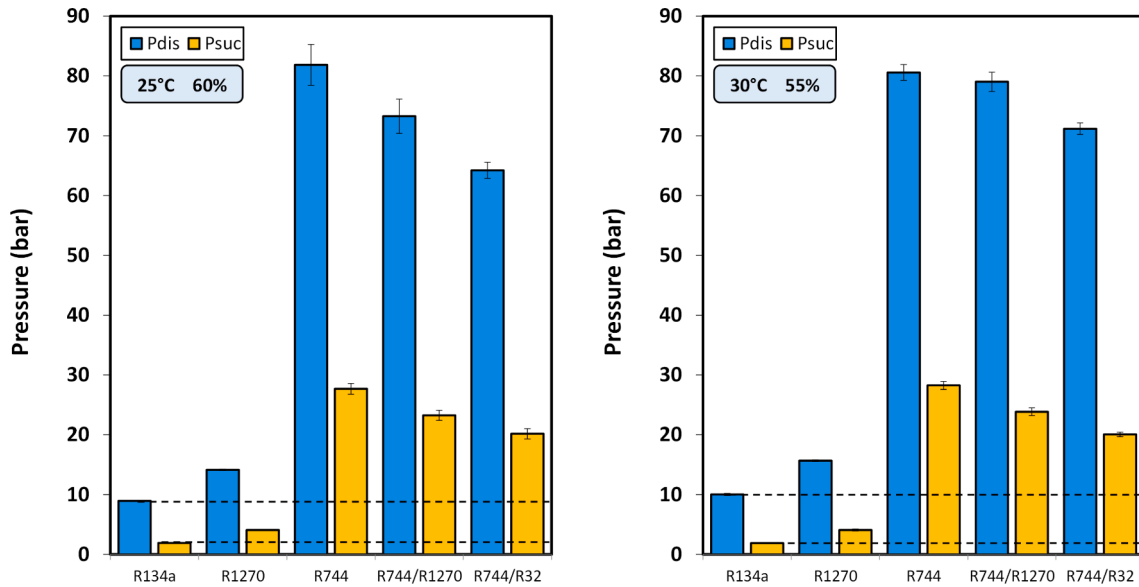
Fig. 10. Average compressor pressures at Class III (left) and Class IV (right) conditions.

4. Experimental analysis

4.1. Mass charge optimization and energy consumption

The mass charge optimization allows determining the optimal refrigerant mass charge by an iterative process using different refrigerant charges. Fig. 7 shows the optimization process including the refrigerant mass charge and the energy consumed by the setup during 16 h of continuous running. Energy consumption is determined using the trapezoidal integration method shown in Eq. (16), where "Ẇ" is the electrical power consumed by the setup, "t" is the acquisition time, and "j" refers to measured data.

$$E = \frac{1}{36 \cdot 10^5} \cdot \int_0^{16h} \dot{W}(t) \cdot dt$$
$$\simeq \frac{1}{36 \cdot 10^5} \cdot \sum_{j=1}^{16h} \left\{ \left[\frac{\dot{W}(j) + \dot{W}(j-1)}{2} \right] \cdot [t(j) - t(j-1)] \right\} \quad (16)$$

Fig. 8 presents the vertical display's energy at the optimal refrigerant mass charge using R134a and R1270 as references. Table 8 gathers the results obtained at these optimal conditions, including reference, operating, and energy parameters. Except for operating conditions, all values are 16 h average values with the corresponding standard deviation. Operating parameters are average values of 40 s before the compressor stops. In total, 89 tests were carried out.

Using pure CO_2 as reference, CO_2-based blends introduce energy savings of up to −17.2 % at 25 °C and up to −8.5 % at 30 °C, as Fig. 8 shows. These savings are higher for $CO_2/R32$ than $CO_2/R1270$,
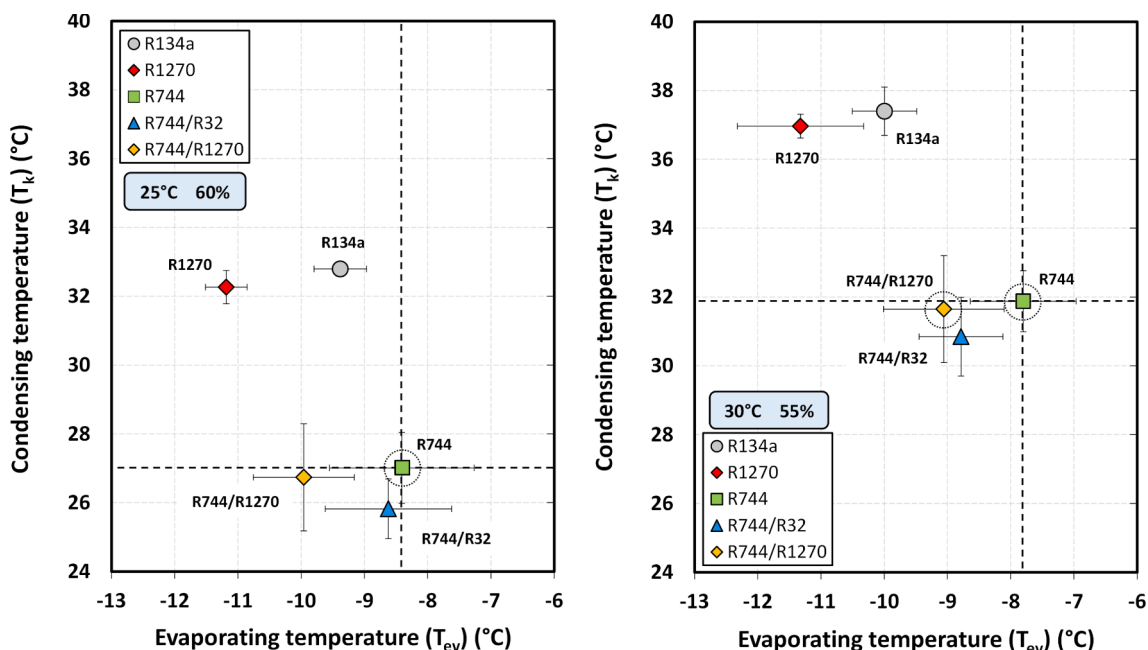

Fig. 11. Average phase-change temperatures at Class III (left) and Class IV (right) conditions.

following the theoretical results presented in Section 2. However, they do not match the COP percentage improvement because energy tests consider non-stationary conditions where time is also included. Therefore, energy tests are essential to determine the global impact of CO_2-based blends.

Compared with R134a, CO_2-blends perform better at both ambient conditions with energy savings of −27.3 % (25 °C) and −8.0 % (30 °C) using the $CO_2/R1270$ mixture, and −28.3 % (25 °C) and −12.1 % (30 °C) utilizing the $CO_2/R32$ blend.

Taking R1270 as the reference, CO_2-blends performs similarly at 25 °C with differences in energy consumption of about + 7.0 % with $CO_2/R32$ and + 8.6 % using $CO_2/R1270$. However, for 30 °C, these differences increase to + 19.2 with $CO_2/R32$ and + 24.8 % utilising the blend of $CO_2/R1270$. The main reason for this increment may be associated with the transcritical (or near-transcritical) operation of the plant. Therefore, the extension of the subcritical range by using mixtures, provides better performance than CO_2 transcritical cycles, especially at lower ambient temperatures.

Regarding the optimum mass charge, it can be noticed that CO_2 blends demand less refrigerant than pure CO_2. For example, using the $CO_2/R32$ blend, the mass charge becomes 9.8 to 14.6 % lower while using $CO_2/R1270$, the reduction is about 11.8 to 15.7 %. For R134a and R1270, the mass charge is lower than CO_2 and blends due to the significant lower vapour and liquid density. In any case, the mass charge for R1270 is lower than the restriction of 150 g fixed by the current IEC 60335–2 regulation.

4.2. Power consumption and Duty-cycle

Since the energy consumption is a combination of electrical power and operating time, Fig. 9 depicts the power consumption of the cooling unit and the compressor's total operating time at the optimal refrigerant mass charge. This last is presented with the *duty-cycle* parameter, which is the relation between the compressor operating time and the total test time (16 h). Because of the high power consumed by the compressor, the variations presented in Fig. 9 are mainly due to this component.

As was expected, the energy savings reached by the alternative CO_2 blends correspond to a reduction in the power consumed by the display unit and the compressor time operation. For the mixture $CO_2/R1270$, the reduction of electrical power varies between −8.3 % (25 °C) to −4.7

% (30 °C), while for $CO_2/R32$, savings move from −14.0 % (25 °C) to −9.1 % (30 °C). Regarding the operating time, both mixtures perform similarly at 25 °C, with −10.2 % less operation on average, and at 30 °C, with −4.5 % savings on average.

Compared with the refrigerant R134a, the mixture $CO_2/R1270$ increases the power consumption from 5.7 % (25 °C) to 3.2 % (30 °C), whilst the $CO_2/R32$ slightly reduces this value up to −1.5 %. However, in terms of duty cycle, both blends report lower operating times, especially at 25 °C, with a maximum reduction of −32.2 %. If hydrocarbon R1270 is taken as a reference, it is evident that it has the minimum power consumption with a duty-cycle very similar at 25 °C but up to 12.0 % lower at 30 °C.

4.3. Operating pressures

Fig. 10 presents the compressor operating pressures summarized in Table 8 for all tested refrigerants, with a clear difference between CO_2-

Table 9
Main parameters during the pull-down process at the optimal mass charge.

| Refrigerant	m_{opt} (g)	T_{env} (°C)	RH_{env} (%)	$T_{prod\ in}$ (°C)	$T_{prod\ fin}$ (°C)	$E_{Pull-down}$ (kW·h)
Class III (25 °C; 60 %)						
$CO_2 / R32$	490	24.9 ± 0.2	60.0 ± 1.9	25.0	3.0	1.18
$CO_2 / R1270$	484	24.9 ± 0.3	59.5 ± 2.7	25.0	3.1	1.19
CO_2	574	25.1 ± 0.3	59.6 ± 2.5	24.8	3.1	1.41
R1270	128	25.2 ± 0.1	60.1 ± 1.5	25.3	3.1	1.08
Class IV (30 °C; 55 %)						
$CO_2 / R32$	460	30.3 ± 0.5	54.0 ± 3.6	30.0	3.1	1.62
$CO_2 / R1270$	450	30.3 ± 0.4	54.2 ± 3.6	30.1	3.1	1.68
CO_2	510	30.3 ± 0.5	53.9 ± 3.6	30.2	3.2	1.73
R134a	242	30.3 ± 0.3	54.5 ± 1.8	30.4	3.0	1.90
R1270	138	30.3 ± 0.5	53.8 ± 1.2	30.3	3.1	1.41
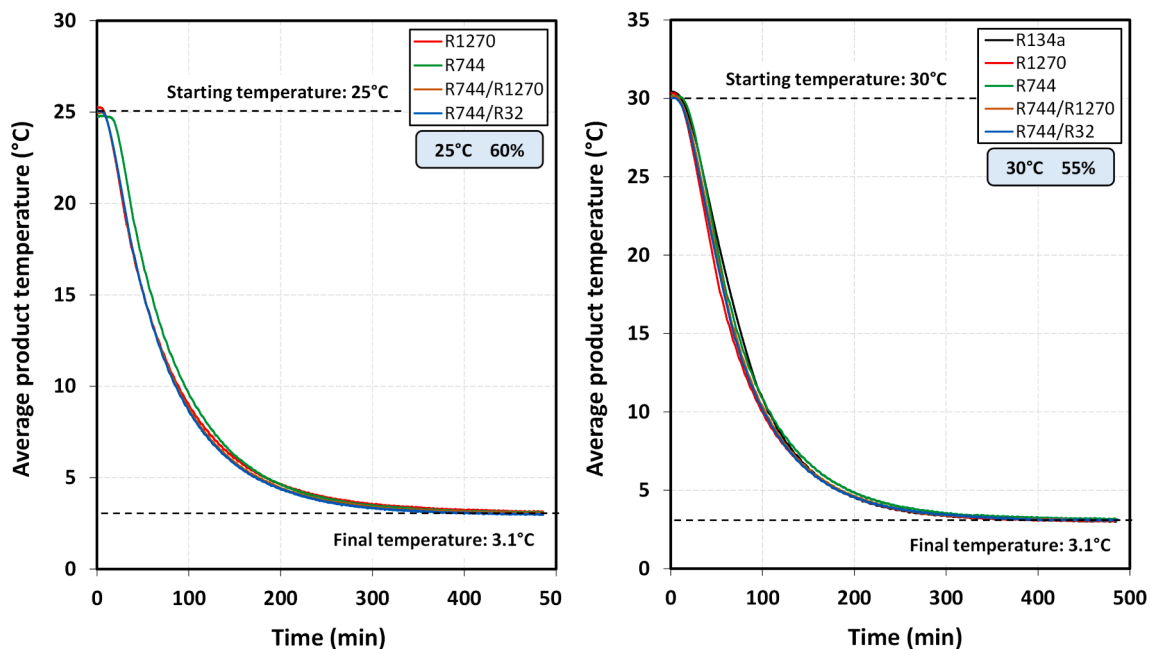
Fig. 12. Pull down tests at Class III (left) and Class IV (right) conditions.
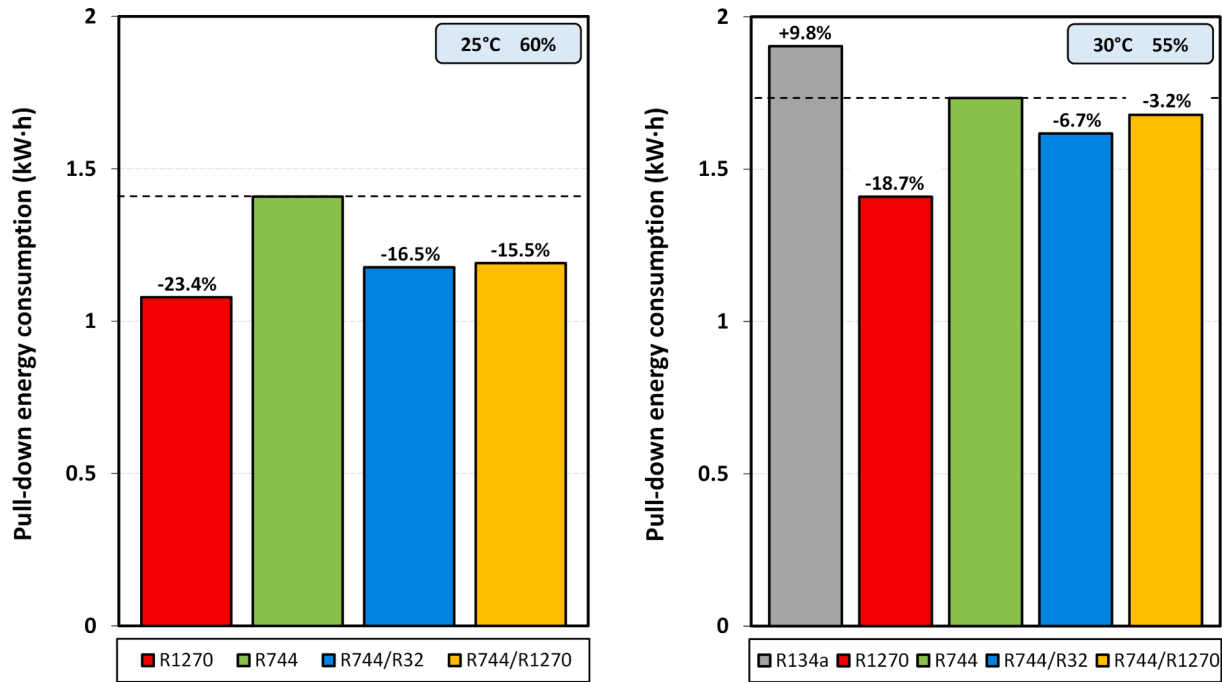
Fig. 13. Energy consumption during the pull down process at Class III (left) and Class IV (right) conditions.

based fluids and the other refrigerants. Thus, taking pure CO_2 as a reference, at 30 °C, the $CO_2/R1270$ mixture reduces the heat rejection pressure to −1.6 bar, while $CO2/R32$ performs at −9.4 bar lower. These reductions are higher at the ambient conditions of 25 °C due to the subcritical operation of blends regarding pure CO_2. At these conditions, the reductions result in −8.6 bar using $CO_2/R1270$ and −17.6 bar with the mixture of $CO_2/R32$.

Regarding the suction pressure, CO_2-based mixtures also reduce this value with decrements ranging from −7.5 bar (25 °C) to −8.2 bar (30 °C) using $CO_2/R32$, and −4.4 bar at both ambient conditions with $CO_2/R1270$. These reductions facilitate the design of components in terms of pressure requirements.

Despite decreasing the pressure levels, the pressure ratio of blends is slightly higher than pure CO_2 and lower than R134a and R1270. Therefore, the values shown in Table 8 may penalize the volumetric and global compressor efficiencies, but further analyses are necessary to confirm this possible effect.

4.4. Operating temperatures

The temperatures used to analyse the operation of tested refrigerants are the phase change temperatures in the condenser and evaporator and the compressor's discharge temperature. Fig. 11 presents the phase-change temperatures evaluated with the mid-point temperature method for zeotropic mixtures using the saturated temperature inlet and outlet of the condenser and evaporator (Eq. (17) and (18), respectively) [59]. Those saturated temperatures are evaluated with the measured pressures and the RefProp® software. For the evaporator, the inlet temperature ($T_{ev\ in}$) is determined by Eq. (19) with the evaporating pressure (P_{ev}) and the inlet enthalpy ($h_{exp\ in}$), assuming an isenthalpic process in the valve.

$$T_k = \frac{T_{k\ vap\ sat} + T_{k\ liq\ sat}}{2} \tag{17}$$

$$T_{ev} = \frac{T_{ev\ vap\ sat} + T_{ev\ in}}{2} \tag{18}$$

$$T_{ev\ in} = f\left(P_{ev}, h_{expin}\right) \tag{19}$$

In transcritical conditions, the condensing temperature corresponds to the temperature at the exit of the gas-cooler. Those values are marked with a circle in Fig. 11.

According to Fig. 11, pure CO_2 performs the highest evaporation temperatures in both ambient conditions, which means that the evaporator's performance is the highest compared with the other refrigerants since the demanding operating conditions are similar in all cases. Furthermore, the CO_2-based blends report lower evaporating temperatures but with a significantly variation due to the effect of the thermostatic expansion valve. Therefore, it is difficult to quantify the deterioration degree, although, on average, the $CO_2/R32$ blend reports a higher evaporation temperature than $CO_2/R1270$. These results are in concordance with those published by Zhu et al. [48] with mixtures of $CO_2/R290$, where the effect of doping CO_2 with R290 reduces the evaporating heat transfer coefficient.

Regarding the condensing temperature, refrigerants R134a and R1270 condensate at an average of + 7.5 K higher than the ambient temperature with a slight variation. Pure CO_2 works in transcritical conditions at both ambient temperatures, so the temperature presented in Fig. 11 corresponds to the gas-cooler exit, which is close to the ambient temperature due to the high thermal effectiveness of the gas-cooler [60]. The CO_2-blends perform even better than pure CO_2 but with high variability, probably due to the glide at the condenser and the transient operation. Except for $CO_2/R1270$ at the ambient temperature of 30 °C that works in transcritical conditions, all cases report a condensing behaviour with an approach to the ambient temperature lower than 2 K.

Finally, the compressor's discharge temperature is measured with a thermocouple installed 10 cm away from the compressor discharge port. The values in Table 8 confirm that hydrocarbon R1270 has the lowest discharge temperature in all conditions, followed by CO_2 at 25 °C and R134a at 30 °C. Regarding the mixtures, $CO_2/R32$ performs the highest discharge temperature with a maximum temperature difference of + 13.7 °C to R1270 and + 6.7 K to pure CO_2. In any case, these values do not penalize the compressor's performance and operation.

4.5. Pull-down analysis

Pull-down tests provide the capacity of the refrigeration unit to cool down the product from the ambient temperature to the desired target conditions. Using the optimum mass charge, nine tests were performed to cool down the product from the ambient conditions of 25 °C and 30 °C to the target product temperature of around 3.1 °C. Fig. 12 depicts the cooling process at both ambient conditions, and Table 9 summarises the main parameters of the pull-down tests.

According to Fig. 12, there are no significant differences in the cooling process nor in total time invested in the pull-down process, so it is difficult to affirm which is the quickest cooling refrigerant. Therefore, to determine the energy consumed unit during pull-down ($E_{Pull-down}$), the time used was counted from the switch on of the refrigerating unit to the defrosting process starting (after 8 h). Fig. 13 compares the energy invested during the pull-down, showing that the defined CO_2-based blends contribute positively to reduce the energy consumption during the pull-down process, allowing significant energy savings compared to pure CO_2. Taking R1270 as a reference, CO_2 blends need, on average, $+9.7$ % more energy at 25 °C and $+16.9$ % at 30 °C to perform the same pull-down. The same effect working with pure CO_2 takes $+30.6$ % and $+23.0$ %, at 25 °C and 30 °C, respectively.

5. Conclusions

This work theoretically and experimentally analyses several CO_2-based binary mixtures maintaining the conditions of GWP above 150 and non-flammability. From the theoretical analysis, the mixtures of $CO_2/R32$, $CO_2/R41$, $CO_2/R1270$, $CO_2/R161$ and $CO_2/R152a$ conduct improvements of COP about $+14.8$ %, $+7.9$ %, $+6.7$ %, $+5.5$ % and $+1.5$ %, respectively, at the optimum operating conditions. These improvements also provide lower optimum heat rejection pressures with reductions from -9.0 bar ($CO_2/R41$) to -18.5 bar ($CO_2/R32$).

The experimental assessment performed with energy tests in a vertical display cooler using the blends of $CO_2/R32$ and $CO_2/R1270$ as *drop-in* of pure CO_2 revealed energy savings of -17.2 % and -16.0 %, respectively, at 25 °C and -8.5 % and -4.3 %, respectively, at 30 °C, regarding pure CO_2. These savings were lower than those obtained using R1270 (-22.6 % at 25 °C and -23.3 % at 30 °C) but higher than the results with R134a in both ambient conditions. The effect on the power consumed by the cooling unit demonstrated that mixtures reduce this value compared to pure CO_2 being so close to the values obtained with R134a. Similar behaviour was obtained with the compressor duty-cycle.

Regarding optimum heat rejection pressure, CO_2-based blends work with lower pressures than CO_2 at the optimized operating conditions with reductions up to -17.6 bar using $CO_2/R32$ and up to -8.6 with $CO_2/R1270$. However, the pressure ratios of blends are slightly higher than pure CO_2.

Concerning operating temperatures, the average evaporating temperature of CO_2 is the highest of all refrigerants, whilst the heat rejection temperature of the mixture $CO_2/R32$ is closest to the ambient temperature compared with the other fluids, including pure CO_2.

Finally, the pull-down process using CO_2-based blends is more efficient than pure CO_2 and, on average, $+9.7$ % energy demanding than R1270 at 25 °C and $+16.9$ % at 30 °C.

Considering the conclusions stated above, the mixtures of $CO_2/R32$ and $CO_2/R1270$ are suggested as an alternative to pure CO_2 with significant reductions in energy, power consumption and working pressures. Furthermore, from the experimental tests campaign, no problems have been detected with those fluids, so they can be used as *drop-ins* in existing transcritical systems or as an alternative to hydrocarbons in those systems where the mass charge exceeds the regulation limits or for security reasons. Notwithstanding, further experimental tests are necessary to prove the theoretical non-flammability of CO_2 blends and a deep leakage analysis to ensure non-flammability in all operating conditions.

CRediT authorship contribution statement

D. Sánchez: Investigation, Methodology, Writing – original draft. **F. Vidan-Falomir:** Data curation, Formal analysis. **L. Nebot-Andrés:** . **R. Llopis:** Supervision. **R. Cabello:** Supervision.

Declaration of Competing Interest

The authors declare that they have no known competing financial interests or personal relationships that could have appeared to influence the work reported in this paper.

Data availability

Data will be made available on request.

Acknowledgements

References

[1] Morlet V., Coulomb D., Dupond J.L. *The impact of the refrigeration sector on climate change. 35th informatory note on refrigeration technologies.* IIR (2017) [on line]. Available on: https://iifiir.org/en/fridoc/the-impact-of-the-refrigeration-sector-on-climate-change-141135 [accessed 12 August 2022].

[2] McLinden MO, Kazakov AF, Brown JS, Domanski PA. A thermodynamic analysis of refrigerants: Possibilities and tradeoffs for Low-GWP refrigerants. Int J Refrig 2014; 38:80–92. https://doi.org/10.1016/j.ijrefrig.2013.09.032.

[3] Sánchez D, Cabello R, Llopis R, Arauzo I, Catalán-Gil J, Torrella E. Energy performance evaluation of R1234yf, R1234ze(E), R600a, R290 and R152a as low-GWP R134a alternatives. Int J Refrig 2017;74:269–82. https://doi.org/10.1016/j.ijrefrig.2016.09.020.

[4] Bell IH, Domanski PA, McLinden MO, Linteris GT. The hunt for nonflammable refrigerant blends to replace R-134a. Int J Refrig 2019;104:484–95. https://doi.org/10.1016/j.ijrefrig.2019.05.035.

[5] Calleja-Anta D, Nebot-Andrés L, Catalán-Gil J, Sánchez D, Cabello R, Llopis R. Thermodynamic screening of alternative refrigerants for R290 and R600a. Results in Engineering 2020;5:100081. https://doi.org/10.1016/j.rineng.2019.100081.

[6] Sánchez D, Cabello R, Llopis R, Catalán-Gil J, Nebot-Andrés L. Energy assessment and environmental impact analysis of an R134a/R744 cascade refrigeration plant upgraded with the low-GWP refrigerants R152a, R1234ze(E), propane (R290) and propylene (R1270). Int J Refrig 2019;104:321–34. https://doi.org/10.1016/j.ijrefrig.2019.05.028.

[7] Kim MH, Pettersen J, Bullard CW. Fundamental process and system design issues in CO_2 vapor compression systems. Prog Energy Combust Sci 2004;30(2):119–74. https://doi.org/10.1016/j.pecs.2003.09.002.

[8] Cabello R, Sánchez D, Patiño J, Llopis R, Torrella E. Experimental analysis of energy performance of modified single-stage CO_2 transcritical vapour compression cycles based on vapour injection in the suction line. Appl Therm Eng 2012;47(5): 86–94. https://doi.org/10.1016/j.applthermaleng.2012.02.031.

[9] Elbel S, Hrnjak P. Flash gas bypass for improving the performance of transcritical R744 systems that use microchannel evaporators. Int J Refrig 2004;27(7):724–35. https://doi.org/10.1016/j.ijrefrig.2004.07.019.

[10] Torrella E, Sánchez D, Llopis R, Cabello R. Energetic evaluation of an internal heat exchanger in a CO_2 transcritical refrigeration plant using experimental data. Int J Refrig 2011;34(1):40–9. https://doi.org/10.1016/j.ijrefrig.2010.07.006.

[11] Tsamos KM, Ge YT, Santosa I, Tassou SA, Bianchi G, Mylona Z. Energy analysis of alternative CO_2 refrigeration system configurations for retail food applications in moderate and warm climates. Energ Conver Manage 2017;150(15):822–9. https://doi.org/10.1016/j.enconman.2017.03.020.

[12] Nebot-Andrés L, Sánchez D, Calleja-Anta D, Cabello R, Llopis R. Experimental determination of the optimum intermediate and gas-cooler pressures of a commercial transcritical CO_2 refrigeration plant with parallel compression. Appl Therm Eng 2021;189(5):116671. https://doi.org/10.1016/j.applthermaleng.2021.116671.

[13] Haida M, Banasiak K, Smolka J, Hafner A, Eikevik TM. Experimental analysis of the R744 vapour compression rack equipped with the multi-ejector expansion work recovery module. Int J Refrig 2016;64:93–107. https://doi.org/10.1016/j.ijrefrig.2016.01.017.

[14] Singh S, Maiya PM, Hafner A, Banasiak K, Neksa P. Energy efficient multiejector CO_2 cooling system for high ambient temperature. Thermal Science and Engineering Progress 2020;19(1):100590. https://doi.org/10.1016/j.tsep.2020.100590.

[15] Bellos E, Tzivanidis C. Enhancing the performance of a CO_2 refrigeration system with the use of an absorption chiller. Int J Refrig 2019;108:37–52. https://doi.org/10.1016/j.ijrefrig.2019.09.009.

[16] Catalán-Gil J, Nebot-Andrés L, Sánchez D, Llopis R, Cabello R, Calleja-Anta D. Improvements in CO_2 Booster Architectures with Different Economizer Arrangements. Energies 2020;13(5).

[17] Casi A, Aranguren P, Araiz M, Sánchez D, Cabello R, Astrain D. Performance assessment of an experimental CO_2 transcritical refrigeration plant working with a thermoelectric subcooler in combination with an internal heat exchanger. Energ Conver Manage 2022;268(15):115963. https://doi.org/10.1016/j.enconman.2022.115963.

[18] Kim SC, Won JP, Kim MS. Effects of operating parameters on the performance of a CO_2 air conditioning system for vehicles. Appl Therm Eng 2009;29(11–12):2408–16. https://doi.org/10.1016/j.applthermaleng.2008.12.017.

[19] Cecchinato L, Corradi M. Transcritical carbon dioxide small commercial cooling applications analysis. Int J Refrig 2011;34(1):50–62. https://doi.org/10.1016/j.ijrefrig.2010.09.019.

[20] Tao YB, He YL, Tao WQ, Wu ZG. Experimental study on the performance of CO_2 residential air-conditioning system with an internal heat exchanger. Energ Conver Manage 2010;51(1):64–70. https://doi.org/10.1016/j.enconman.2009.08.024.

[21] Yelishala S.C. *Thermodynamic and combustion study on blends of hydrocarbons and carbon dioxide as alternative refrigerants*. PhD-Thesis (2019). Department of Mechanical and Industrial Engineering. Northeastern University. Boston, Massachusetts 10.17760/D20324058.

[22] Sobieraj M, Rosiński M. Experimental study of the heat transfer in R744/R600a mixtures below the R744 triple point temperature. Int J Refrig 2019;103:243–52. https://doi.org/10.1016/j.ijrefrig.2019.03.038.

[23] Di Nicola G, Giuliani G, Polonara F, Stryjek R. Blends of carbon dioxide and HFCs as working fluids for the low-temperature circuit in cascade refrigerating systems. Int J Refrig 2005;28:130–40. https://doi.org/10.1016/j.ijrefrig.2004.06.014.

[24] Niu B, Zhang Y. Experimental study of the refrigeration cycle performance for the R744/R290 mixtures. Int J Refrig 2007;30(1):37–42. https://doi.org/10.1016/j.ijrefrig.2006.06.002.

[25] Kim JH, Cho JM, Kim MS. Cooling performance of several CO_2/propane mixtures and glide matching with secondary heat transfer fluid. Int J Refrig 2008;31(5):800–6. https://doi.org/10.1016/j.ijrefrig.2007.11.009.

[26] Onaka Y., Miyara A., Tsubaki K., Koyama S. *Analysis of heat pump cycle using CO_2/DME mixture refrigerant*. International Refrigeration and Air Conditioning Conference (2008). Paper 956. http://docs.lib.purdue.edu/iracc/956.

[27] Cox N., Mazur V., Colbourne D. *New high pressure low-GWP azeotropic and near-azeotropic refrigerant blends*. International Refrigeration and Air Conditioning Conference (2008). Paper 987. http://docs.lib.purdue.edu/iracc/987.

[28] Sarkar J, Bhattacharyya S. Assessment of blends of CO_2 with butane and isobutane as working fluids for heat pump applications. Int J Therm Sci 2009;48:1460–5. https://doi.org/10.1016/j.ijthermalsci.2008.12.002.

[29] Di Nicola G, Polonara F, Stryjek R, Arteconi A. Performance of cascade cycles working with blends of CO_2 + natural refrigerants. Int J Refrig 2011;34(6):1436–45. https://doi.org/10.1016/j.ijrefrig.2011.05.004.

[30] Fan X, Zhang X, Wang F. Simulation study on a heat pump system using R744/R290 as refrigerant. J Civil Eng Archit 2013;7(2):220–6. https://doi.org/10.17265/1934-7359/2013.02.011.

[31] Dai B, Dang C, Li M, Tian H, Ma Y. Thermodynamic performance assessment of carbon dioxide blends with low-global warming potential (GWP) working fluids for a heat pump water heater. Int J Refrig 2015;56:1–14. https://doi.org/10.1016/j.ijrefrig.2014.11.009.

[32] Jemni N, Elakhdar M, Nehdi E, Kairouani L. Performance investigation of cascade refrigeration system using CO_2 and mixtures. Int J Air-Condition Refrig 2015;23(3):1550022. https://doi.org/10.1142/S2010132515500224.

[33] Bouteiller P., Terrier M.F., Tobaly P. *A methodology and bench design for experimental study of heat pump thermodynamic cycles using CO_2 based mixtures*. 12th IIR- Gustav Lorentzen Natural Working Fluids Conference, Edinburgh (2016). Paper 1015. DOI:10.18462/iir.gl.2016.1015.

[34] Nasruddin, Sholahudin S., Giannetti N., Arnas. Optimization of a cascade refrigeration system using refrigerant C_3H_8 in high temperature circuits (HTC) and a mixture of C_2H_6/CO_2 in low temperature circuits (LTC). Appl Thermal Eng (2016) 104: 96-103. http://dx.doi.org/10.1016/j.applthermaleng.2016.05.059.

[35] Bouteiller P, Terrier MF, Tobaly P. Experimental study of heat pump thermodynamic cycles using CO_2 based mixtures - methodology and first results. AIP Conf Proc 2017;1814:020052. https://doi.org/10.1063/1.4976271.

[36] Wang D, Lu Y, Tao L. Thermodynamic analysis of CO_2 blends with R41 as an azeotropy refrigerant applied in small refrigerated cabinet and heat pump water heater. Appl Therm Eng 2017;125:1490–500. https://doi.org/10.1016/j.applthermaleng.2017.07.009.

[37] Tobaly P., Terrier M.F., Bouteiller P. *CO_2 + propane mixture as working fluid for refrigeration in hot climates. experimental results of energy efficiency tests*. 13th IIR- Gustav Lorentzen Natural Working Fluids Conference, Valencia (2018). Paper 1276. DOI: 10.18462/iir.gl.2018.1276.

[38] Yu B, Wang D, Liu C, Jiang F, Shi J, Chen J. Performance improvements evaluation of an automobile air conditioning system using CO_2-propane mixture as a refrigerant. Int J Refrig 2018;88:172–81. https://doi.org/10.1016/j.ijrefrig.2017.12.016.

[39] Ju F, Fan X, Chen Y, Ouyang H, Kuang A, Ma S, et al. Experiment and simulation study on performances of heat pump water heater using blend of R744/R290. Energ Build 2018;169:148–56. https://doi.org/10.1016/j.enbuild.2018.03.063.

[40] Yu B, Yang J, Wang D, Shi J, Guo Z, Chen J. Experimental energetic analysis of CO_2/R41 blends in automobile air conditioning and heat pump systems. Appl Energy 2019;239:1142–53. https://doi.org/10.1016/j.apenergy.2019.02.028.

[41] Kumar K., Kumar P. *Analysis of Propane + CO_2 mixture as a working fluid in a vapor compression refrigeration system*. 8th Conference on Ammonia and CO_2 Refrigeration Technology, Ohrid, North Macedonia (2019). Paper 0043. http://dx.doi.org/10.18462/iir.nh3-co2.2019.0043.

[42] Massuchetto L.H.P., do Nascimento R.B.C., de Carvalho S.M.R., de Araújo H.V., d'Angelo J.V.H. *Thermodynamic performance evaluation of a cascade refrigeration system with mixed refrigerants: R744/R1270, R744/R717 and R744/RE170*. International Journal of Refrigeration (2019) 106: 201-212. 10.1016/j.ijrefrig.2019.07.005.

[43] Sun Z, Cui Q, Wang Q, Ning J, Guo J, Dai B, et al. Experimental study on CO_2/R32 blends in a water-to-water heat pump system. Appl Therm Eng 2019;162:114303. https://doi.org/10.1016/j.applthermaleng.2019.114303.

[44] Sánchez D., Cabello R., Llopis R., Catalán-Gil J., Nebot-Andrés L., Calleja-Anta D., Gil E. *Energy improvements in a stand-alone transcritical refrigeration system using a low-GWP mixture of CO_2/R1270*. 25th IIR International Congress of Refrigeration. Montréal, Canada (2019). Paper 123. http://dx.doi.org/10.18462/iir.icr.2019.1231.

[45] Sobieraj M. Development of novel wet sublimation cascade refrigeration system with binary mixtures of R744/R32 and R744/R290. Appl Therm Eng 2021;196:117336. https://doi.org/10.1016/j.applthermaleng.2021.117336.

[46] Xie J, Wang J, Lyu Y, Wang D, Peng X, Liu H, et al. J Therm Anal Calorim 2021;147:6883–92. https://doi.org/10.1007/s10973-021-11011-x.

[47] Zhang XP, Wang F, Fan XW, Wei XL, Wang FK. Determination of the optimum heat rejection pressure in transcritical cycles working with R744/R290 mixture. Appl Therm Eng 2013;54:176–84. https://doi.org/10.1016/j.applthermaleng.2013.02.006.

[48] Zhu Y, Wu X, Wei Z. Heat transfer characteristics and correlation for CO_2/propane mixtures flow evaporation in a smooth mini tube. Appl Therm Eng 2015;81:253–61. https://doi.org/10.1016/j.applthermaleng.2015.02.009.

[49] DeAngelis J.M., Hrnjak P.S., *Experimental study of system performance improvements in transcritical R744 systems with applications to bottle coolers*. Air Conditioning and Refrigeration Center (ACRC). University of Illinois (2005). Reference: ACRC CR-57. [on line]. Available on: https://hdl.handle.net/2142/13416 [accessed 12 August 2022].

[50] ASHRAE, Standard 34-2019. Designation and safety classification of refrigerants (2019).

[51] Calm J. M. *ARTI refrigerant database. Data summaries - Volume 1: single-compound refrigerants*. Air-Conditioning and Refrigeration Technology Institute (1999). Reference: DOE/CE/23810-105. [on line]. Available on: https://www.ahrinet.org/App_Content/ahri/files/RESEARCH/Technical%20Results/MCLR-Program/ARTI%20Refrigerant%20Database%20Data%20summaries-Volume%20One-Single-compound%20Refrigerants-Calm-1999-DOE-CE-23810-105.pdf [accessed 12 August 2022].

[52] IPCC. *Climate Change 2014: Synthesis Report. Contribution of Working Groups I, II and III to the Fifth Assessment Report of the Intergovernmental Panel on Climate Change* [Core Writing Team, R.K. Pachauri and L.A. Meyer (eds.)]. IPCC, Geneva, Switzerland (2014).

[53] Schroeder V. *Calculation of flammability and lower flammability limits of gas mixtures for classification purposes*. Bundesanstalt für Materialforschung und –prüfung (BAM). Division "Gases, Gas Plants" (2016). [on line]. Available on: https://opus4.kobv.de/opus4-bam/frontdoor/deliver/index/docId/41830/file/Schroeder++Calculation+of+Flammability+Limits.pdf [accessed 12 August 2022].

[54] Kondo S, Takizawa K, Takahashi A, Tokuhashi K. Extended Le Chatelier's formula for carbon dioxide dilution effect on flammability limits. J Hazard Mater 2006;A138:1–8. https://doi.org/10.1016/j.jhazmat.2006.05.035.

[55] Sánchez D, Andreu-Nácher A, Calleja-Anta D, Llopis R, Cabello R. Energy impact evaluation of different low-GWP alternatives to replace R134a in a beverage cooler. Experimental analysis and optimization for the pure refrigerants R152a, R1234yf, R290, R1270, R600a and R744. Energ Conver Manage 2022;256(15):115388. https://doi.org/10.1016/j.enconman.2022.115388.

[56] Sánchez D, Catalán-Gil J, Cabello R, Calleja-Anta D, Llopis R, Nebot-Andrés L. Experimental analysis and optimization of an R744 Transcritical cycle working with a mechanical subcooling system. Energies 2020;13(12):3204. https://doi.org/10.3390/en13123204.

[57] Alabdulkarem A, Eldeeb R, Hwang Y, Aute V, Radermacher R. Testing, simulation and soft-optimization of R410A low-GWP alternatives in heat pump system. Int J Refrig 2015;60:106–17. https://doi.org/10.1016/j.ijrefrig.2015.08.001.

[58] Cabello R, Sánchez D, Llopis R, Andreu-Nácher A, Calleja-Anta D. Energy impact of the Internal Heat Exchanger in a horizontal freezing cabinet. Experimental evaluation with the R404A low-GWP alternatives R454C, R455A, R468A, R290 and R1270. Int J Refrig 2022;137:22–33. https://doi.org/10.1016/j.ijrefrig.2022.02.007.

[59] ASERCOM, *Refrigerant glide and effect on performances declaration*. ASERCOM Guideline (2015). [on line]. Available on: https://asercom.org/wp-content/uploads/2021/01/Refrigerant-Glide-and-Effect-on-Performances-Declaration.pdf [accessed 12 August 2022].

[60] Sánchez D, Cabello R, Llopis R, Torrella E. Development and validation of a finite element model for water – CO_2 coaxial gas-coolers. Appl Energy 2012;93:637–47. https://doi.org/10.1016/j.apenergy.2011.12.100.